Hindawi
Journal of Spectroscopy
Volume 2024, Article ID 2585610, 10 pages
https://doi.org/10.1155/2024/2585610

Research Article

Collaborative Inversion of Soil Water Content in Alpine Meadow Area Based on Multitemporal Polarimetric SAR and Optical Remote Sensing Data

Meng Kong, Xiaoqing Zuo, and Yongfa Li

Department of Surveying and Mapping, Institute of Land and Resources Engineering, Kunming University of Science and Technology, Kunming 650000, China

Correspondence should be addressed to Meng Kong; 851617350@qq.com

Received 25 November 2023; Revised 20 December 2023; Accepted 23 December 2023; Published 24 January 2024

Academic Editor: Naveen Mishra

Soil water content is a critical environmental parameter in research and practice, though various technological and contextual constraints limit its estimation in arid areas with vegetation cover. This study combined the multitemporal remote sensing data of Sentinel-1 and Landsat 8 to conduct an inversion study on surface soil water content under low vegetation cover in Nagqu, central Tibetan Plateau. Four vegetation indices (NDVI, ARVI, EVI, and RVI) were extracted from optical remote sensing data. A water cloud model was used to eliminate the influence of the vegetation layer on the backscattering coefficient associated with vegetation cover, and a predictive model suitable for the Nagqu area was constructed. The water cloud model effectively incorporated a vegetation index instead of vegetation water content. We found that VV polarization was more suitable for soil water content inversion than VH polarization. Among the four vegetation indices, the soil water content inversion model constructed with RVI under VV polarization had the best fit ($R^2 = 0.8212$; RMSE = 6.30). The second-best fit was observed for vegetation water content-NDVI ($R^2 = 0.8201$). The soil water content inversion models all had an $R^2 > 0.6$, regardless of the vegetation index used, though the RVI had the best fitting effect, indicating that this vegetation index is highly applicable in the water cloud model, as a substitute for vegetation water content, and is expected to perform well in similar study sites.

1. Introduction

Soil water content (soil moisture) is not only a basic condition for plant growth but is also an important environmental parameter in the fields of ecology, hydrology, agriculture, and climate change and a useful indicator for drought monitoring and crop yield estimation, among others. It is one of the most important parameters for characterizing ground surfaces [1, 2]. Therefore, large-scale monitoring of soil water content is not only an important part of agricultural research and the evaluation of environmental factors but also of great importance for developing regional and global climate mitigation strategies and predicting regional dry and wet conditions.

Traditional soil water content monitoring is mainly conducted using established specialized monitoring or meteorological stations. Although this method has high accuracy, it is limited by a small detection range, low turnover, and data representativeness and requires considerable resources [3–5]. With the maturation of satellite remote sensing technology, multisource remote sensing can generate large-scale soil water content estimates with high spatial and temporal resolution, facilitating the acquisition of dynamic real-time information and compensating for the shortcomings of traditional monitoring methods [6].

Techniques for soil water content inversion using remote sensing are mainly categorized into optical remote sensing inversion, microwave remote sensing inversion, and collaborative inversion [7–9]. Optical remote sensing inversion is performed by extracting sensitive information related to soil water content from optical remote sensing images. According to the different extraction approaches, it can be divided into the reflectivity, index, and thermal inertia methods [10]. Optical remote sensing cannot directly provide spectral information for soil in densely vegetated areas and is mainly applicable to the inversion of bare surfaces. Compared with optical remote sensing, microwave remote sensing, categorized as active or passive according to the working method of the sensor, has the advantages of not being affected by weather, strong penetration, and all-weather capabilities [11–13]. Passive microwave remote sensing inverts the soil water content using a prediction model established with soil radiation temperature (obtained using the microwave radiometer) and measured soil data [14–16]. Active microwave remote sensing, which is less affected by interference, is based on the mathematical relationship between the backscattering coefficient and soil water content, among which the linear regression model is the most commonly used [17–19]. The radar backscattering coefficient of active microwave remote sensing is mainly affected by the soil dielectric constant, surface roughness, and vegetation cover. In the vegetation-covered area, the scattering and attenuation effect of the vegetation layer on the radar backscatter echo will reduce the sensitivity of the backscatter coefficients to the change in soil water content, thus affecting the accuracy of the inversion. Therefore, the effect of the vegetation cover on the backscatter coefficients needs to be eliminated.

Vegetation index can provide information about vegetation growth status and cover, so vegetation index can be used instead of vegetation cover. At the same time, the relationship between different types of vegetation index and soil water content may be different. Therefore, understanding the applicability of vegetation index is helpful to better select the soil water content inversion model suitable for specific regions and environments, so as to improve the accuracy and reliability of soil water content inversion. Alternatively, the sensitivity of optical remote sensing to vegetation information can be used to extract relevant vegetation canopy information, and the influence of the vegetation layer can be eliminated by water cloud [20] or MIMICS models [21], which enable collaborative inversion with microwave remote sensing and improve the inversion accuracy of soil moisture in vegetation-covered areas. For example, Liu et al. [22] combined Sentinel-1A and -2A images, used the water cloud model to remove the influence of the vegetation layer, and then estimated soil moisture in the farmland area using machine learning. Rawat et al. [23] estimated soil moisture by combining the soil's dielectric constant properties with the radar backscattering coefficient obtained using the SA schemes of RISAT-1 data. Su and Cao [24] used full-polarization data to invert soil moisture using AIEM, water cloud, and MIMICS models according to land use types and vegetation in different rocky desert areas.

Our study locality, Nagqu City, Tibet, is located at high altitudes with a cold and dry climate, making drought an important factor affecting agricultural production. An effective inversion method can improve the monitoring of soil water content and enable the dissemination of this crucial information to producers at all levels within this region. In this study, multitemporal remote sensing images with a large time span were used for collaborative inversion of soil water content. Given the unique context of this study locality, we explored the applicability of the vegetation index instead of vegetation water content to further improve drought detection capabilities in this region. .

2. Materials and Methods

2.1. Study Area. The Nagqu soil temperature and humidity observation network in the central Qinghai-Tibet Plateau is located within a 100×100 km area (91.5°–92.5°E, 31°-32°N, Figure 1) at an average altitude of 4650 m above sea level. Most of the selected sites were located in the central and northern parts of Nagqu County, and a few were located southeast of Amdo County and southwest of Nyainrong County. It belongs to the high-altitude subcold climate zone, where the total annual hours of sunshine are 2852.6–2881.7, annual average temperature is −0.9 to −3.3°C, annual average relative humidity is 48–51%, and the annual average precipitation is 380 mm. Most of the study area is located in the pure summer and autumn pastoral area of Nagqu. The vegetation type is a typical alpine meadow belt, mainly composed of wormwood meadows. The grass layer has a height of 1–5 cm and total annual growth days of 150–170 d, indicating that the withering period is longer than the growing period and vegetation cover is generally low.

2.2. Data Sources

2.2.1. Remote Sensing Data. Sentinel-1, a follow-up satellite of ERS-2 and Envisat, is an important component of the European Space Agency's Copernicus Program (previously known as GMES) and integral to the Earth observation program. The constellation comprises Sentinel-1A and Sentinel-1B satellites equipped with a C-band synthetic aperture radar (SAR) at an orbital altitude of 693 km. The observation period of a single satellite is 12 d, and the combined observation of two satellites is 6 d. Sentinel-1 has four imaging modes, SMStripmap (SM), interferometric wide swath (IW), extrawide swath (EW), and wave mode (WV). The GRD data in the IW mode were selected for this study. The obtained SAR image comprised L1 data with a spatial resolution of 5×20 m, with VV and VH dual polarization (Table 1). The downloaded image data were subjected to orbit correction, thermal noise removal, radiometric calibration, multiview, filtering, terrain correction, and decibel processing in the ESA SNAP. We used Refined Lee filtering to obtain the total backscattering coefficient of the radar.

Landsat 8 is an Earth observation satellite jointly launched by the National Aeronautics and Space Administration (NASA) and the United States Geological Survey (USGS) on February 11, 2013, carrying two sensors, a land imager (OLI) and a thermal infrared sensor (TIRS). The OLI

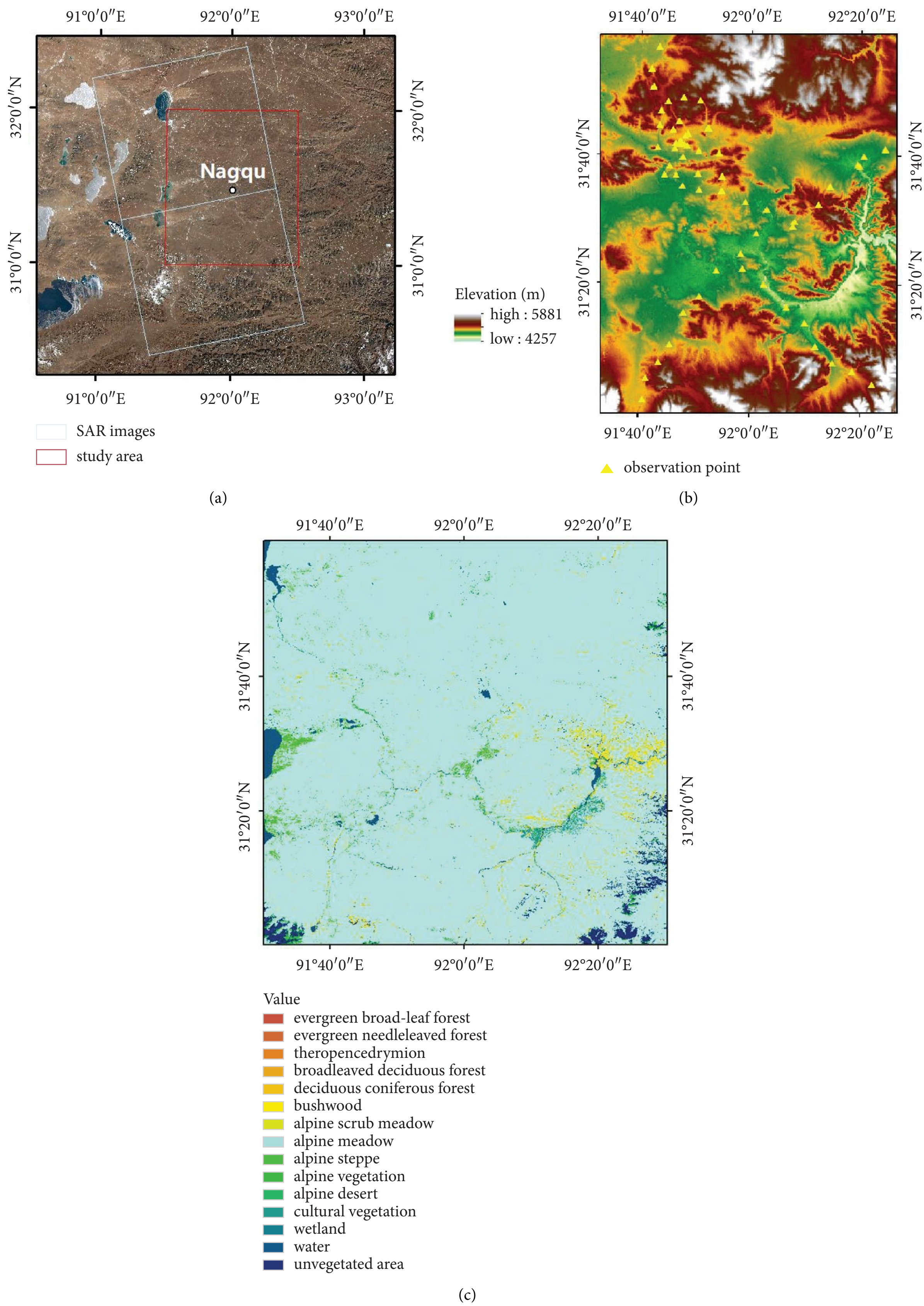

Figure 1: Location of the study area (a), distribution of monitoring points (b), and vegetation types (c).

Table 1: Sentinel-1 SAR images acquired for the study area.

ID	Acquisition date	Mean incidence angle (°)	Imaging model	Polarization	Resolution (m)
D1	2021-01-28	44.36	IW	VV/VH	10
D2	2020-12-11	44.36	IW	VV/VH	10
D3	2020-10-24	44.36	IW	VV/VH	10
D4	2020-01-10	44.36	IW	VV/VH	10
D5	2018-12-22	44.36	IW	VV/VH	10
D6	2017-12-03	44.36	IW	VV/VH	10

includes nine bands and the TIRS includes two thermal infrared bands. Optical images from the same day as the SAR data were downloaded from the USGS website (https://earthexplorer.usgs.gov). Landsat 8 L2 SP T1-level OLI data were used to calculate the normalized difference vegetation index (NDVI), enhanced vegetation index (EVI), ratio vegetation index (RVI), and atmospheric impedance index (ARVI) in ENVI 5.6 to obtain the corresponding grid image (Table 2).

To promote the accuracy of the model, we selected optical and microwave remote sensing images for the same date; the cloud content of the optical remote sensing images was 5%.

2.2.2. Soil Water Content Data. The soil water content data were obtained from the multiscale observation network of soil temperature and moisture on the central Tibetan Plateau provided by the National Tibetan Plateau Data Center [25, 26], which mainly considers soil water content in the surface layer (0–5 cm) at 57 monitoring stations. By screening and eliminating abnormal data from six image datasets, our final dataset considers data for 178 monitoring points for the construction and verification of the remote sensing image inversion model.

2.3. Analytical Approaches

2.3.1. Quantification of Soil Water Content. Soil water content is usually expressed as soil weight water content, soil volumetric water content, and relative soil water content. Soil weight water content refers to the weight ratio of soil water to dried soil. The soil volumetric water content refers to the volumetric ratio of soil water per unit of soil. Relative soil water content refers to the percentage of soil water content relative to field capacity.

The soil water content data obtained in this study reflected soil weight water content; therefore, we converted the data to soil volumetric water content using the following formula:

$$m_v = m_q \times \rho, \quad (1)$$

where m_v is the soil volumetric water content (%), m_q is the soil weight water content (%), and ρ is the soil bulk weight ($g{\cdot}cm^{-3}$).

2.3.2. Optical and Microwave Remote Sensing Collaborative Inversion Method. We observed a linear correlation between the soil backscattering coefficient and soil water content, according to which the soil water content inversion model can be established as follows:

$$m_v = a \times \delta^0_{\text{soil}} + b, \quad (2)$$

where m_v is the soil volumetric water content (%), δ^0_{soil} is the soil backscattering coefficient (dB), and a and b are the empirical parameters.

2.3.3. Water Cloud Model. The scattering and attenuation effects of the vegetation layer cause partial reflection of the signal received by the sensor. To eliminate the influence of the vegetation layer on the inversion of soil water content in areas with vegetation cover, we applied the water cloud model proposed by Baghdadi et al. [18], which is often used to invert soil water content in areas with low vegetation cover [27, 28]. The water cloud model divides the total received radar backscatter coefficient (δ^0_{total}) into two parts, the soil scattering coefficient through the vegetation (δ^0_{soil}) and the vegetation scattering coefficient (δ^0_{veg}), and is modeled as

$$\delta^0_{\text{total}} = \delta^0_{\text{veg}} + \gamma^2 \delta^0_{\text{soil}}, \quad (3)$$

$$\delta^0_{\text{veg}} = A \times \text{VWC} \times \left(1 - \gamma^2\right) \times \cos(\theta), \quad (4)$$

$$\gamma^2 = \text{EXP}\,(-2 \times B \times \text{VWC} \times \sec(\theta)). \quad (5)$$

The collation can be deduced as

$$\delta^0_{\text{soil}} = \frac{\delta^0_{\text{total}} - A \times \text{VWC} \times \left(1 - \gamma^2\right) \times \cos(\theta)}{\text{EXP}\,(-2 \times \text{B} \times \text{VWC} \times \sec(\theta))}. \quad (6)$$

In equations (3)–(6), δ^0_{total} is the total radar backward scattering coefficient (dB), δ^0_{veg} is the vegetation layer backward scattering coefficient (dB), δ^0_{soil} is the soil backward scattering coefficient (dB), γ^2 is the two-time attenuation factor of the vegetation scattering coefficient (%), VWC is the vegetation water content ($g{\cdot}cm^{-3}$), θ is the radar incidence angle (°), and A and B are the empirical vegetation parameters.

Table 2: Landsat 8 images acquired for the study area.

ID	Acquisition date	Sensor	Resolution (m)
D1	2021-01-28	OLI	30
D2	2020-12-11	OLI	30
D3	2020-10-24	OLI	30
D4	2020-01-10	OLI	30
D5	2018-12-22	OLI	30
D6	2017-12-03	OLI	30

As the study area is dominated by alpine meadows, the empirical parameters A and B were set to 0.0014 and 0.084, respectively, according to Bindish and Barros [29] (Table 3).

2.3.4. Estimation of Vegetation Water Content. Vegetation water content is an important parameter in water cloud models and can be inverted using optical remote sensing data based on three methods: spectral reflectivity, spectral index, and radiative transfer model methods. The spectral index method has a higher accuracy than the reflectivity method and is simpler than the radiative transfer method; therefore, it is more widely used [30].

The NDVI and normalized difference water index (NDWI) are commonly used to estimate vegetation water content using water cloud models. To explore the feasibility of different vegetation indices for characterizing the VWC in the water cloud model, we first calculated a reference vegetation water content estimate using the empirical relationship between the NDVI and VWC established by Jackson and Gao et al. [31, 32]. With the formula,

$$\mathrm{VWC}_{\mathrm{NDVI}} = 0.098 \times e^{4.225\mathrm{NDVI}}. \tag{7}$$

Second, the EVI, RVI, and atmospherically resistant vegetation index (ARVI) were directly substituted into the vegetation water content parameter in the water cloud model to invert the soil water content. Compared to the $\mathrm{VWC}_{\mathrm{NDVI}}$ inversion, these vegetation indices were calculated as follows:

$$\begin{aligned}
\mathrm{NDVI} &= \frac{\rho_{\mathrm{NIR}} - \rho_{\mathrm{RED}}}{\rho_{\mathrm{NIR}} + \rho_{\mathrm{RED}}},\\
\mathrm{EVI} &= 2.5 \times \frac{\rho_{\mathrm{NIR}} - \rho_{\mathrm{RED}}}{\rho_{\mathrm{NIR}} + 6\rho_{\mathrm{RED}} - 7.5\rho_{\mathrm{blue}} + 1},\\
\mathrm{RVI} &= \frac{\rho_{\mathrm{NIR}}}{\rho_{\mathrm{RED}}},\\
\mathrm{ARVI} &= \frac{\rho_{\mathrm{NIR}} - \left(2\rho_{\mathrm{RED}} - \rho_{\mathrm{blue}}\right)}{\rho_{\mathrm{NIR}} + \left(2\rho_{\mathrm{RED}} + \rho_{\mathrm{blue}}\right)}.
\end{aligned} \tag{8}$$

2.3.5. Accuracy Evaluation of Model. We evaluated the accuracy of the inversion model of soil water content using goodness of fit (R^2) and root mean square error (RMSE), which can be calculated as follows:

$$\begin{aligned}
R^2 &= \frac{\sum_{I=1}^{N}\left(\hat{y}_i - \overline{y}\right)^2}{\sum_{I=1}^{N}\left(y_i - \overline{y}\right)^2},\\
\mathrm{RMSE} &= \sqrt{\frac{\sum_{I=1}^{N}\left(\hat{y}_i - y_i\right)^2}{n}},
\end{aligned} \tag{9}$$

where $\hat{y}_i$ is the inversion value of soil water content (%), $\overline{y}$ is the mean soil water content (%), y_i is the measured value of soil water content (%), and n is the number of samples used in verification.

R^2 represents the fitting relationship between the inversion and measured values; the closer it is to 1, the better the fit of the model. RMSE represents the degree of deviation between the inversion and measured values; the smaller the value, the better the fit of the model.

In this study, the vegetation index and backscattering coefficient in satellite images of six time-phases are extracted, respectively, and the soil backscattering coefficient is solved by using the water cloud model to eliminate the influence of vegetation cover. There are a total of 178 available monitoring point data, each time-phase of about 30 data. Then, the empirical parameters a and b are solved by linear fitting the measured data of some monitoring points with the soil backscattering coefficient. Finally, the remaining measured data are brought into the constructed inversion model to detect its accuracy.

The technical workflow for inverting soil water content is shown in Figure 2.

3. Results and Discussion

3.1. Analysis of Soil Water Content Collaborative Inversion Results. Previous studies reported a correlation between the radar backscattering coefficient and soil water content [33]. Simultaneously, different polarization modes are affected by vegetation cover to varying degrees, resulting in different polarization modes and soil water content correlations [34, 35].

According to the above principles and processes, data from 100 monitoring points in the reference dataset were selected to construct the inversion model, and the remaining 78 data points were used to verify the accuracy of the model. The ratio of validation set to test set allocation is approximately 3 : 4. Firstly, the vegetation index and backscatter coefficient of 178 monitoring points were calculated by

Table 3: Parameter values of A and B under different vegetation types.

Parameters	Synthesis	Grazing	Winter wheat	Grassland
A	0.0012	0.0009	0.0018	0.0014
B	0.0910	0.0320	0.1380	0.0840

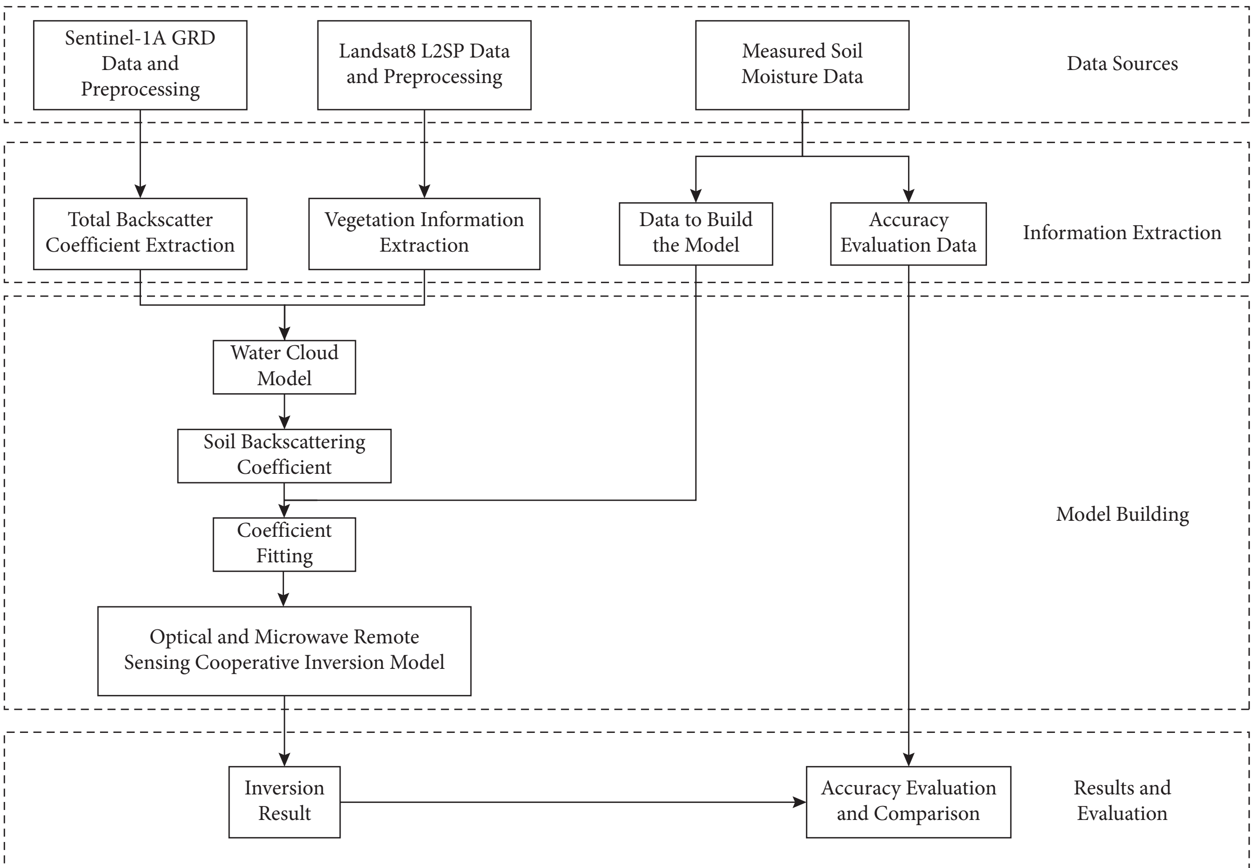

Figure 2: Workflow of soil water content inversion.

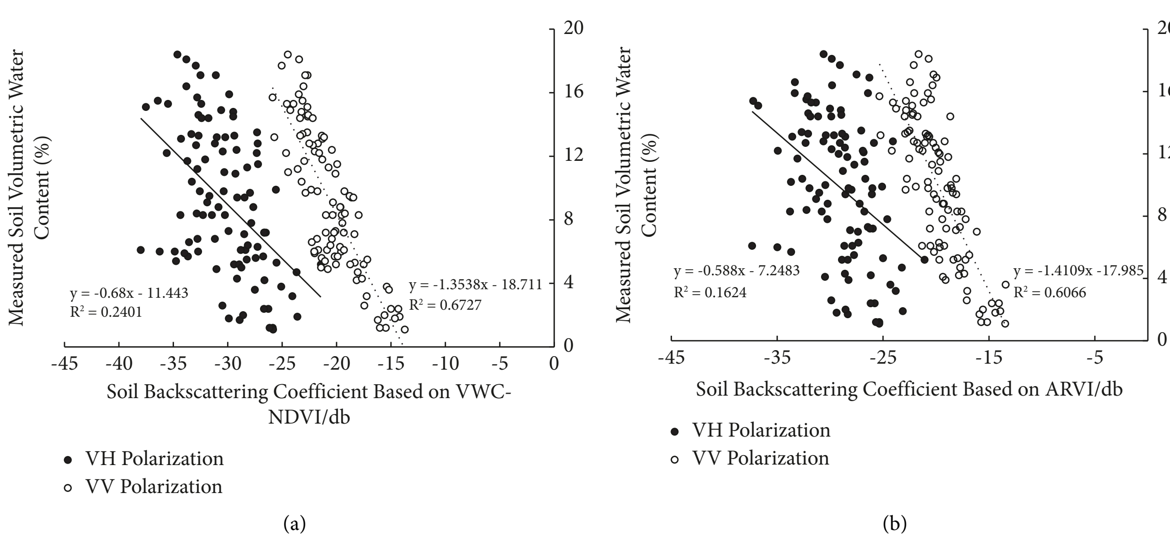

Figure 3: Continued.

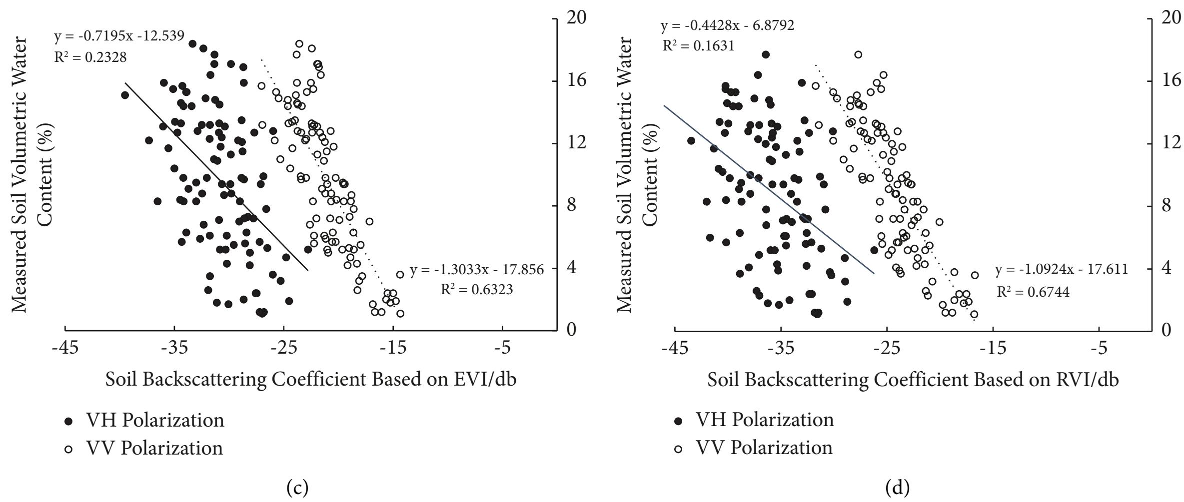

Figure 3: Fitting relationship between soil backscatter coefficient based on VWC-NDVI (a), ARVI (b), EVI (c), and RVI (d) and measured soil volumetric water content under VV/VH polarization.

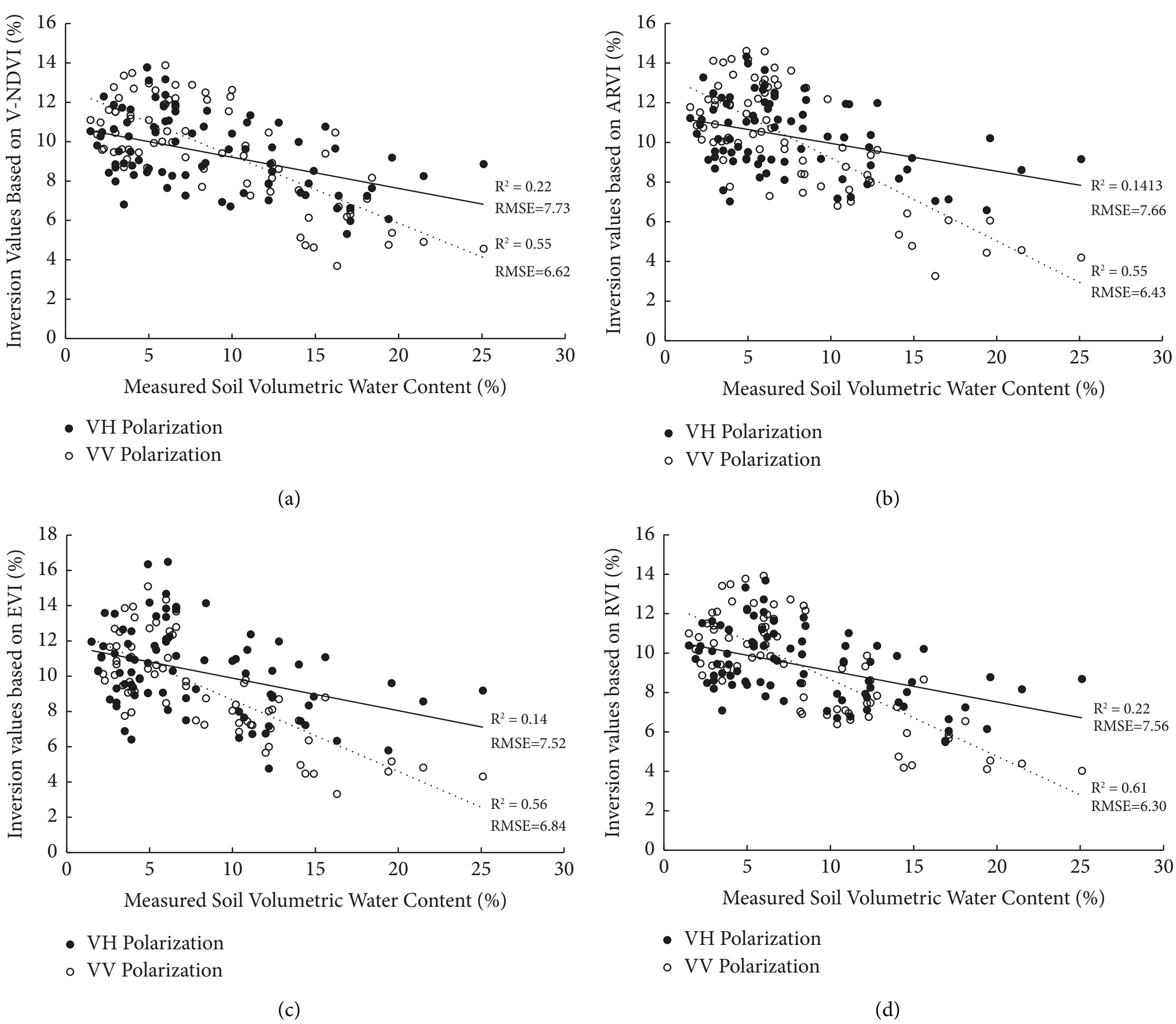

Figure 4: Relationship between soil water content inversion value based on VWC-NDVI (a), ARVI (b), EVI (c), and RVI (d) and measured soil volumetric water content.

optical image and SAR, respectively, and the soil backscattering coefficient is extracted by using the water cloud model to eliminate the influence of vegetation cover. Then, the solved soil backscattering coefficient is linearly fitted with 100 measured data. The fitting results of 100 measured soil water content and soil backscattering coefficient under VV/VH dual polarization are shown in Figure 3. The fitting degree of vegetation water content and vegetation index on the soil backscattering coefficient and measured soil water content under VH polarization was lower than that under VV polarization (Figure 3). This indicates that the ability of microwaves to penetrate the vegetation layer under VV polarization is stronger than that under VH polarization, which is consistent with previous results. Meanwhile, the accuracy of the model constructed varied with different parameters for vegetation water content. Under VV polarization, the soil backscattering coefficients based on VWC-NDVI and RVI best fit with the measured soil water content data ($R^2 = 0.6727$ and 0.6744, respectively). EVI corresponded with the second-best fit ($R^2 = 0.6323$), while ARVI corresponded with the worst fit ($R^2 = 0.6066$). Under VH polarization, the soil backscattering coefficient and soil water content based on VWC-NDVI had the best fitting effect ($R^2 = 0.2401$), while ARVI had the worst fitting effect ($R^2 = 0.1624$). The analysis showed that the fitting effect was better with the RVI than with the vegetation water content estimated by VWC-NDVI, indicating that RVI can directly replace the vegetation water content parameter in the model. The goodness of fit associated with EVI and ARVI was also above $R^2 > 0.6$, indicating good model fit and applicability.

3.2. Verification of Soil Water Content Inversion Accuracy. The accuracy of the inversion model was verified using the dataset composed of the remaining 78 monitoring points based on goodness of fit (R^2) and root mean square error (RMSE). The soil backscattering coefficients of 78 monitoring points were substituted into the above four linear models to invert the soil water content. Then, the inversion value of soil water content is linearly fitted with the measured value. We observed a good fit between the backscattering coefficients and soil water content after removing the influence of vegetation using VV and VH dual polarization (Figure 4), which is consistent with previous results [36]. Consistent with our findings in Section 3.1, we observed a better fit under VV polarization than under VH polarization. Under VV polarization, the RMSE did not vary much between models with different vegetation indices (the maximum was 6.84 for EVI and the minimum was 6.30 for RVI); however, we observed a large difference in R^2 (the maximum value was 0.61 for RVI and the minimum value was 0.55 for VWC-NDVI and ARVI). Considering the degree of fitting and the need for accurate prediction of the inversion value, the linear regression model $y = -1.0924x - 17.611$ based on RVI in Figure 3(d) has the best predictive performance for soil water content estimation and is most suitable for the study area.

4. Conclusions

In this study, the NDVI, ARVI, EVI, and RVI were calculated using multitemporal data from Sentinel-1 GRD and Landsat 8. The influence of the vegetation layer was eliminated by using a water cloud model. Based on the model fit associated with the different vegetation indices, we constructed a predictive model for soil water content inversion in vegetation-covered areas and made the following conclusions:

(1) Using Sentinel-1 and Landsat 8 remote sensing data for collaborative inversion, we found that the model fit and accuracy were better under VV polarization than those under VH polarization, proving that VV polarization was more suitable for soil moisture inversion in this area.

(2) ARVI, EVI, and RVI were selected to replace the vegetation water content parameter in the inversion model, and all had R^2 values >0.6, indicating a good fitting effect. RVI performed better than VWC-NDVI ($R^2 = 0.6744$), suggesting that it can effectively replace vegetation water content in the water cloud model.

(3) By calculating NDVI, ARVI, EVI, and RVI and using the corresponding empirical relationship formula to convert NDVI to VWC-NDVI as a reference, we found that using different vegetation parameters to invert or replace vegetation water content can improve the water cloud model performance and enhance the accuracy of soil water content inversion to different extents.

We effectively applied NDVI, ARVI, EVI, and RVI to the collaborative inversion of soil water content. RVI had the best fitting effect, which may be related to the hilly and mountainous surface characteristics of the study area in Nagqu. We therefore propose that RVI is especially applicable in mountainous study sites, where it can eliminate various terrain effects to improve inversion accuracy.

Note that there are some limitations to our study. The data provided by Sentinel-1 are in the VH dual polarization mode, while research on the HH polarization mode is lacking. Therefore, future studies should analyze the applicability of the remaining two polarization modes to obtain better inversion results. Although the vegetation layer and soil roughness greatly affect the radar backscattering coefficient, we only considered the effect of scattering from the vegetation layer on the inversion of soil water content.

Therefore, subsequent studies could benefit from applying soil roughness to the inversion model, which may further improve model accuracy at our and comparable study sites.

Data Availability

The data that support the findings of this study are openly available in the National Tibetan Plateau Data Center at (https://doi.org/10.11888/Terre.tpdc.271918) and (https://doi.org/10.11888/Terre.tpdc.272408).

Conflicts of Interest

The authors declare that there are no conflicts of interest regarding the publication of this article.

Acknowledgments

This research was funded by the National Natural Science Foundation of China (Grant no. 42161067). The National Natural Science Foundation of China is from the Kunming University of Science and Technology, so the authors are very grateful to the school for the cultivation of our students. At the same time, the authors also appreciate the open source data provided by the National Tibetan Plateau Data Center and ASF so that the authors could carry out this study smoothly.

References

[1] A. S. Sagayaraj, S. K. Kabilesh, D. Mohanapriya, and A. Anandkumar, "Determination of soil moisture content using image processing-A Survey," in *Proceedings of the 2021 6th International Conference on Inventive Computation Technologies (ICICT)*, pp. 1101–1106, IEEE, Coimbatore, India, January 2021.

[2] G. G. Ponnurangam, T. Jagdhuber, I. Hajnsek, and Y. S. Rao, "Soil moisture estimation using hybrid polarimetric SAR data of RISAT-1," *IEEE Transactions on Geoscience and Remote Sensing*, vol. 54, no. 4, pp. 2033–2049, 2016.

[3] D. Zhang and G. Zhou, "Estimation of soil moisture from optical and thermal remote sensing: a review," *Sensors*, vol. 16, no. 8, p. 1308, 2016.

[4] J. Xue, Z. Li, Q. Feng, J. Gui, and B. Zhang, "Spatiotemporal variations of water conservation and its influencing factors in ecological barrier region, Qinghai-Tibet Plateau," *Journal of Hydrology: Regional Studies*, vol. 42, Article ID 101164, 2022.

[5] K. Uddin, M. A. Matin, and F. J. Meyer, "Operational flood mapping using multi-temporal Sentinel-1 SAR images: a case study from Bangladesh," *Remote Sensing*, vol. 11, no. 13, p. 1581, 2019.

[6] B. Fu, Y. Liang, Z. Lao et al., "Quantifying scattering characteristics of mangrove species from Optuna-based optimal machine learning classification using multi-scale feature selection and SAR image time series," *International Journal of Applied Earth Observation and Geoinformation*, vol. 122, Article ID 103446, 2023.

[7] X. Qin, Z. Pang, and W. Jiang, "Research progress and challenges of soil moisture optical remote sensing inversion method," *People's Pearl River*, vol. 42, no. 11, pp. 38–45+111, 2021.

[8] K. Das and P. K. Paul, "Present status of soil moisture estimation by microwave remote sensing," *Cogent Geoscience*, vol. 1, Article ID 1084669, 2015.

[9] B. Barrett and G. P. Petropoulos, "Satellite remote sensing of surface soil moisture," *Remote sensing of energy fluxes and soil moisture content*, vol. 85, pp. 85–119, 2013.

[10] T. Ishida, H. Ando, and M. Fukuhara, "Estimation of complex refractive index of soil particles and its dependence on soil chemical properties," *Remote Sensing of Environment*, vol. 38, no. 3, pp. 173–182, 1991.

[11] L. I. Zhanjie, J. Chen, Y. Liu, X. Yao, and J. Yu, "Soil moisture retrieval from remote sensing," *Journal of Beijing Normal University*, vol. 56, pp. 474–481, 2020.

[12] Y. Bao, L. Lin, S. Wu, K. A. Kwal Deng, and G. P. Petropoulos, "Surface soil moisture retrievals over partially vegetated areas from the synergy of Sentinel-1 and Landsat 8 data using a modified water-cloud model," *International Journal of Applied Earth Observation and Geoinformation*, vol. 72, pp. 76–85, 2018.

[13] M. A. Teng, L. Han, and Q. Liu, "Improved water cloud model inversion of surface soil water content in Spanish farmland considering surface roughness," *Journal of Agricultural Engineering*, vol. 35, no. 24, pp. 129–135, 2019.

[14] P. C. Dubois, J. Van Zyl, and T. Engman, "Measuring soil moisture with imaging radars," *IEEE Transactions on Geoscience and Remote Sensing*, vol. 33, no. 4, pp. 915–926, 1995.

[15] T. J. Jackson, "III. Measuring surface soil moisture using passive microwave remote sensing," *Hydrological Processes*, vol. 7, no. 2, pp. 139–152, 1993.

[16] E. G. Njoku, T. J. Jackson, V. Lakshmi, T. K. Chan, and S. Nghiem, "Soil moisture retrieval from AMSR-E," *IEEE Transactions on Geoscience and Remote Sensing*, vol. 41, no. 2, pp. 215–229, 2003.

[17] F. T. Ulaby, A. Aslam, and M. C. Dobson, "Effects of vegetation cover on the radar sensitivity to soil moisture," *IEEE Transactions on Geoscience and Remote Sensing*, no. 4, pp. 476–481, 1982.

[18] N. Baghdadi, N. Holah, and M. Zribi, "Soil moisture estimation using multi-incidence and multi-polarization ASAR data," *International Journal of Remote Sensing*, vol. 27, no. 10, pp. 1907–1920, 2006.

[19] M. Zribi, N. Baghdadi, and C. Guérin, "Analysis of surface roughness heterogeneity and scattering behavior for radar measurements," *IEEE Transactions on Geoscience and Remote Sensing*, vol. 44, no. 9, pp. 2438–2444, 2006.

[20] E. P. W. Attema and F. T. Ulaby, "Vegetation modeled as a water cloud," *Radio Science*, vol. 13, no. 2, pp. 357–364, 1978.

[21] F. T. Ulaby, K. Sarabandi, K. Y. L. E. Mcdonald, M. Whitt, and M. C. Dobson, "Michigan microwave canopy scattering model," *International Journal of Remote Sensing*, vol. 11, no. 7, pp. 1223–1253, 1990.

[22] Y. Liu, J. Qian, and H. Yue, "Combined Sentinel-1A with Sentinel-2A to estimate soil moisture in farmland," *Ieee Journal of Selected Topics in Applied Earth Observations and Remote Sensing*, vol. 14, pp. 1292–1310, 2021.

[23] K. S. Rawat, V. K. Sehgal, S. Pradhan, and S. S. Ray, "Retrieval and validation of soil moisture from FRS-1 data set of radar imaging satellite (RISAT-1)," *Arabian Journal of Geosciences*, vol. 10, no. 20, pp. 445–510, 2017.

[24] C. Su and Y. Cao, "Research on inversion of soil moisture in karst area based on full-polarization SAR data," *IEEE Access*, vol. 9, pp. 117512–117519, 2021.

[25] K. Yang, Y. Y. Chen, L. Zhao et al., *Multiscale Observation Network Data Set for Soil Temperature and Moisture in the*

Central Tibetan Plateau (2010-2021), National Tibetan Plateau Science Data Center, Beijing, China, 2021.

[26] G. Zhou, H. Ren, T. Liu et al., *Vegetation Map of Qinghai Tibet Plateau in 2020 with 10 M Spatial Resolution*, National Tibetan Plateau Data Center, Beijing, China, 2022.

[27] D. Han, S. Liu, Y. Du et al., "Crop water content of winter wheat revealed with Sentinel-1 and Sentinel-2 imagery," *Sensors*, vol. 19, no. 18, p. 4013, 2019.

[28] S. Rabiei, E. Jalilvand, and M. Tajrishy, "A method to estimate surface soil moisture and map the irrigated cropland area using sentinel-1 and sentinel-2 data," *Sustainability*, vol. 13, no. 20, Article ID 11355, 2021.

[29] R. Bindlish and A. P. Barros, "Parameterization of vegetation backscatter in radar-based, soil moisture estimation," *Remote Sensing of Environment*, vol. 76, no. 1, pp. 130–137, 2001.

[30] J. Luo, J. Qiu, T. Zhao, and D. Wang, "Sentinel-1 based soil moisture estimation in middle reaches of heihe river basin," *Remote Sensing Technology and Application*, vol. 35, pp. 23–32, 2020.

[31] T. J. Jackson, D. Chen, M. Cosh et al., "Vegetation water content mapping using Landsat data derived normalized difference water index for corn and soybeans," *Remote Sensing of Environment*, vol. 92, no. 4, pp. 475–482, 2004.

[32] Y. Gao, J. P. Walker, M. Allahmoradi, A. Monerris, D. Ryu, and T. J. Jackson, "Optical sensing of vegetation water content: a synthesis study," *Ieee Journal of Selected Topics in Applied Earth Observations and Remote Sensing*, vol. 8, no. 4, pp. 1456–1464, 2015.

[33] F. Ulaby, "Radar measurement of soil moisture content," *IEEE Transactions on Antennas and Propagation*, vol. 22, no. 2, pp. 257–265, 1974.

[34] J. Lei, W. Yang, and X. Yang, "Soil moisture in a vegetation-covered area using the improved water cloud model based on remote sensing," *Journal of the Indian Society of Remote Sensing*, vol. 50, pp. 1–11, 2022.

[35] S. Paloscia, S. Pettinato, E. Santi, C. Notarnicola, L. Pasolli, and A. J. R. S. O. E. Reppucci, "Soil moisture mapping using Sentinel-1 images: algorithm and preliminary validation," *Remote Sensing of Environment*, vol. 134, pp. 234–248, 2013.

[36] S. Bousbih, M. Zribi, M. El Hajj et al., "Soil moisture and irrigation mapping in A semi-arid region, based on the synergetic use of Sentinel-1 and Sentinel-2 data," *Remote Sensing*, vol. 10, no. 12, p. 1953, 2018.